Acta Derm Venereol 2014; 94: 14–19

INVESTIGATIVE REPORT

Distribution and Quantitation of Skin Iron in Primary Haemochromatosis: Correlation with Total Body Iron Stores in Patients Undergoing Phlebotomy

Teresa PINHEIRO[1], Raquel SILVA[2], Rita FLEMING[3], Afonso GONÇALVES[4], Maria A. BARREIROS[5], João N. SILVA[2], Patrice MORLIÈRE[6], René SANTUS[7] and Paulo FILIPE[2]

[1]IST-ITN, Instituto Superior Técnico, Universidade Técnica de Lisboa & Centro de Física Nuclear, Sacavém, [2]Clínica Universitária de Dermatologia, Hospital de Santa Maria & Faculdade de Medicina, Universidade de Lisboa, [3]Serviço Imunohemoterapia, [4]Serviço Radiologia, Hospital de Santa Maria, [5]LNEG, UES, Lisbon, Portugal, [6]INSERM, U1088, and Université de Picardie Jules Verne, Faculté de Médecine et de Pharmacie, Amiens, and [7]Département RDDM, Muséum National d'Histoire Naturelle, Paris, France

Measurement of the concentration of iron in the skin, if correlated with total body iron stores, may enable better informed decisions on when to initiate, change or stop therapy in hereditary heamochromatosis. Naïve haemochromatosis patients with iron overload and with C282Y and/or H63D HFE mutations were evaluated at the following time-points: disease diagnosis, end of the therapy programme, and 6 months after the end of therapy. The distribution and concentration of iron in the skin were assessed by quantitative nuclear microscopy methods, in parallel with serum and plasma iron concentration. Iron content in the liver was determined by nuclear magnetic resonance. Iron accumulated in the epidermis; its concentration increased from outer to inner layers, being maximal in the basal layer (7.33 ± 0.98 µmol/g). At all 3 time-points, most of the iron was associated with the extracellular space. During the phlebotomy programme the iron content of the skin and the liver decreased by a factor of 2. These data suggest that measurements of iron concentration in the epidermis, which is a readily accessible tissue, reflect iron overload in the liver. ***Key words: skin; iron distribution; haemochromatosis; proton microscopy.***

Accepted Jan 25, 2013; Epub ahead of print May 27, 2013

Acta Derm Venereol 2014; 94: 14–19.

Teresa Pinheiro, IST/ITN, Instituto Superior Técnico, Universidade Técnica de Lisboa, E.N. 10, 2685-953 Sacavém, Portugal. E-mail: murmur@itn.pt

Hereditary haemochromatosis (HH) is a disease caused by increased intestinal absorption of iron, resulting in its accumulation in multiple organs, such as the liver, heart, pancreas (1, 2) and skin (3), causing fibrosis and affecting their function. It is generally agreed that the C282Y and H63D mutations of the *HFE* gene are responsible for hereditary haemochromatosis (1), and both mutations are presently considered in HH screening. The C282Y mutation modifies the structure of the HFE protein, abrogating its association with the transferrin receptor and causing iron storage overload (4). The physiological role of the H63D mutation is less studied, although *in vitro* studies have shown that the affinity between the transferrin receptors and Fe-transferrin is reduced (4). Large population studies have shown that both the compound heterozygous and homozygous H63D genotypes have much lower penetrance than the C282Y homozygous genotype (1, 2). In the haemochromatosis phenotype, hyper-ferritinaemia, transferrin saturation (1,5) and increased hepatic iron concentration (6) are associated with H63D homo- or hetero-zygosity as observed with C282Y homozygotes or C282/H63D.

The diagnosis of haemochromatosis is based on genetic testing and indirect serological markers (7), which may not accurately reflect tissue overload of iron, as they can be influenced by other clinical conditions (8). Although non-invasive magnetic resonance imaging (MRI) of the liver is often sufficient to assess the iron overload status, some cases require confirmation by invasive hepatic biopsy (9, 10).

However, invasive techniques are not appropriate for serial observations and follow-up during periodic phlebotomies (7), which limits iron availability to tissues by removing iron from the circulation. Thus, new indicators and strategies to provide direct or indirect information on organ iron overload are needed. Because of its accessibility, skin is an organ of choice in this context. Helpful cross-sectional and longitudinal information can be obtained readily regarding the amount of iron deposition during a given time period and the clearance of iron from parenchymatous tissues by therapy intervention. Detailed studies on distribution and quantitation of iron in the skin in patients with HH have however not yet been carried out. There are few reports on iron distribution in normal human skin (11, 12), in patients with thalassaemia (13), and in animal models (14, 15).

The main objective of the present study was therefore to assess the appropriateness of skin as an indicator of organ iron deposition, and of therapy efficacy, by measuring iron concentration in the skin, in combination with conventional blood tests, plasma and serum iron concentrations, and the concentration of iron in the liver assessed by MRI.

 doi: 10.2340/00015555-1601
 ISSN 0001-5555

MATERIALS AND METHODS

Patients

A total of 28 patients, over 18 years of age, with elevated iron levels (18 men and 10 women; mean age ± SD 50 ± 14 years) diagnosed with HH for the first time were enrolled in the study (demographic, biological and resonance data from patients at diagnosis are shown in Table SI[1]). All patients were diagnosed on the basis of the usual clinical and biochemical data and the most frequent mutations on the *HFE* gene. Recommended biochemical blood tests for screening of haemochromatosis were performed, including serum ferritin (Ferr), transferrin saturation (TS) and total iron-binding capacity (TIBC). Blood cells, platelets counts, glycaemia and liver function evaluation were also performed. Liver iron content (LIC) was measured by quantitative MRI. The patients were either symptomatic or asymptomatic. They underwent phlebotomy therapy weekly (as tolerated) along with therapy for other relevant co-morbidities, such as cirrhosis, hepatocarcinoma, hepatitis C virus infection, diabetes mellitus, porphyria cutanea tarda, and steatohepatitis (Table SI[1]). The number of phlebotomies, volume of blood withdrawn per course, treatment duration, and total amount of iron removed during the therapy programme, varied according to the patient's condition. During treatment, patients underwent dietary adjustment. The clinical results were evaluated by following the evolution of blood iron indicators, with the aim of reaching ferritin levels of 50–100 ng/ml.

Study design

Patients were assessed at 3 time-points: Phase 1: at disease diagnosis, prior to phlebotomy therapy; Phase 2: at the end of the phlebotomy therapy programme; and Phase 3: 6 months after stopping the therapy programme.

Biochemical blood tests, LIC and determinations of iron content in the skin were performed in all patients before starting the therapy programme, at the end of the therapy programme, and during follow-up. Measurements performed during the pre-therapeutic and subsequent phases were synchronized. Informed consent was obtained for all subjects, in accordance with the Declaration of Helsinki, and the study was approved by the local ethics committee.

Sampling and methods

Blood samples were collected by venipuncture. Serum and plasma were separated by centrifugation (2,500 rpm, 10 min) and stored at –80ºC.

Skin was obtained by a 3-mm diameter punch biopsy from the lumbar-sacral region. Biopsies were quench-frozen in liquid nitrogen and stored at –80ºC until processing. Only one biopsy at a time was taken from each patient. Sections 14-µm thick were cut from the frozen biopsy in a cryostat at –25ºC (Cryotome 620E, Thermo Shandon, Cheshire, UK), dried and mounted in specific frames, as described elsewhere (16).

Serum iron concentration (S-Fe) was determined by the standard colorimetric method (together with TIBC determination), and plasma iron concentration (P-Fe) was determined by total reflection X-ray fluorescence (17).

Distribution and concentration profiles of iron in transverse sections of cryopreserved skin samples were compiled by nuclear microscopy using a combination of 3 techniques (16): (*i*) particle-induced X-ray emission (PIXE), (*ii*) Rutherford backscattering spectroscopy (RBS), and (*iii*) scanning transmission ion microscopy (STIM). This method has the unique capability of providing real-time morphological images and maps of multiple elements above sodium in the periodic table and, simultaneously, to quantify them down to the level of parts per million.

Nuclear microscopy was performed in the "Ion Beam Laboratory" of the IST/ITN. A focused 2.0 MeV proton beam with a spot size of 2–3 µm was used to scan across a selected area of interest of the skin cryosection. Data from the 3 techniques were obtained simultaneously. Images of the sample density were obtained by STIM and used to identify skin morphology. The concentration of iron was determined by PIXE with high quantitative accuracy and with a sensitivity of approximately 1 µg/g in biological material, such as tissue sections and cells. The concentration of matrix constituents was obtained by RBS. The distribution images of Fe were superimposed on the density images. Consequently, Fe concentrations can be associated directly with morphological details of the skin. Concentration profiles were obtained by analysing a sequential number of points (corresponding approximately to the focused beam area) along a transept of the scanned skin section. Skin cryo-sections were analysed in vacuum, and iron concentrations in the skin were expressed in µmol/g on a dry weight basis.

System characteristics, data acquisition, and the method for calculation of concentration have been described previously (16).

MRI was performed at the Radiology Service of Hospital de Santa Maria, with a 0.5-T Gyroscan T5-NT system (Philips Medical System, Best, The Netherlands). The MRI results were analysed by an experienced radiologist. Briefly, the MRI technique consists of 3 gradient echo sequences (T1, proton density, and long-echo time sequence T2) following the protocol established by Gandon et al. (18). This protocol is based on a T2-weighted gradient-recalled-echo, GRE sequence, which was found to be the most sensitive, allowing the detection of clinically relevant liver iron overload greater than 60 µmol/g, with 89% sensitivity and 80% specificity, and was validated with biochemical measures of hepatic iron concentration (18). The repetition time (TR), echo time (TE) and pulse angle used in the gradient echo sequences to obtain the T1, proton density and T2 images were: T1: 120 ms, 14 ms, 90º; proton density: 120 ms, 14 ms, 20º; and T2: 120 ms, 28 ms, 20º, respectively. To assess possible hepatic lesions the whole liver was first inspected using T1-weighted spin-echo (T1-SE) sequence. Afterwards, 6 magnetic resonance sections were taken for each sequence and one of the sections chosen to evaluate the signal intensity (SI), in order to avoid global variations in SI between images. The SI in the hepatic parenchyma was measured in 3 regions of interest > 1 cm^2 and in the paraspinal muscles in 2 regions of interest. After calculating the mean of the measurements, the liver-to-muscle SI ratio was calculated for each sequence and these values inputted to the program for calculation of LIC (available at the University of Rennes Website; www.radio.univ-rennes1.fr). This calculation was performed for all patients.

Statistical analysis

Statistical analysis of the data included a χ^2 test to compare categorical variables, and non-parametric Mann–Whitney test to compare continuous variables. Differences between treatment phases were calculated with non-parametric Wilcoxon pair test. Correlations between iron concentration in the skin and blood test values were examined by Spearman's correlation coefficient using rank and linear regression analyses. A linear mixed-effects regression model was used to fit the phase-dependent iron content variations in the liver and skin, taking sex, age, co-morbidities and genotype into consideration as confounders. The model took into account that, for each patient, the mea-

[1]https://doi.org/10.2340/00015555-1601

surements at 3 different time-points are associated. To comply with normality requirements, iron concentration variables were log-transformed.

Values of $p < 0.05$ (two-tailed) were considered statistically significant. Calculations were performed using SPSS (version 17.0) and R (version 2.7.0) software packages.

RESULTS

Iron distribution in the skin

Fig. 1 shows images of transversal cryo-sections of skin obtained by nuclear microscopy techniques with spatial resolution of approximately 2 μm. By measuring the energy loss of each ion impinging at each position in the scanned area, an image can be formed that represents the mass distribution within the tissue. Mass density images of selected skin regions evidenced morphological details (Fig. 1A) that can easily be associated with histological features. By measuring the emitted X-rays from the iron atoms present in the tissue, an image of the distribution of the element is also produced (Fig. 1B). Superposition of the distribution with the mass density map allows determination of the exact location of the element. Fig. 1C shows that the iron concentration increases from the stratum corneum (where iron levels were lowest) to the inner layers, peaking at the basal layer and decreasing in the papillary dermis. For comparison, data extracted from healthy skin is also shown in Fig. 1C. A similar iron distribution profile is observed, which agrees with that reported in previous studies (16, 19).

Skin iron changes during treatment and follow-up

The iron concentrations during therapy were examined in the major strata, i.e. the stratum corneum (SC), stratum spinosum (SP), basal layer (BL), and papillary dermis (PD). Iron concentrations were also measured in total epidermis (EPI) by combining the data for all epidermal strata, and in superficial skin (SSK) by combining the data for the epidermis and papillary dermis. Results obtained for patients with HH are summarized in Table SII[1]), which also reports data from healthy skin.

At Phase 1, when compared to control values, iron levels were significantly augmented in all skin regions with the exception of SC (Table I). After stopping the phlebotomy programme (Phase 2) skin iron content dropped drastically and continued to decrease until Phase 3. However, control levels were reached only at Phase 2 in SP and at Phase 3 in BL. At Phase 3, high iron levels were still measured in PD, EPI and SSK.

During therapy and 6 months after the end of the phlebotomies, the iron content measured in SC, SP and BL strata decreased to control values, but the iron levels in SSK and its major components, EPI and PD, remained significantly augmented. By contrast, no change in SC iron levels is observed during the 3 evaluation phases when compared with controls.

Iron distribution at the cellular level

Using the high-resolution mass density images, and taking advantage of the small beam size, epidermal cells can be visualized and the iron profiles of cells obtained. Extracellular and intracellular iron content can therefore be measured. Due to the complexity of the analysis, a sub-set of 6 patients with HH was randomly selected. The analysis was performed only in cryosections where basal keratinocytes could be individualized. In addition, cryosections were inspected

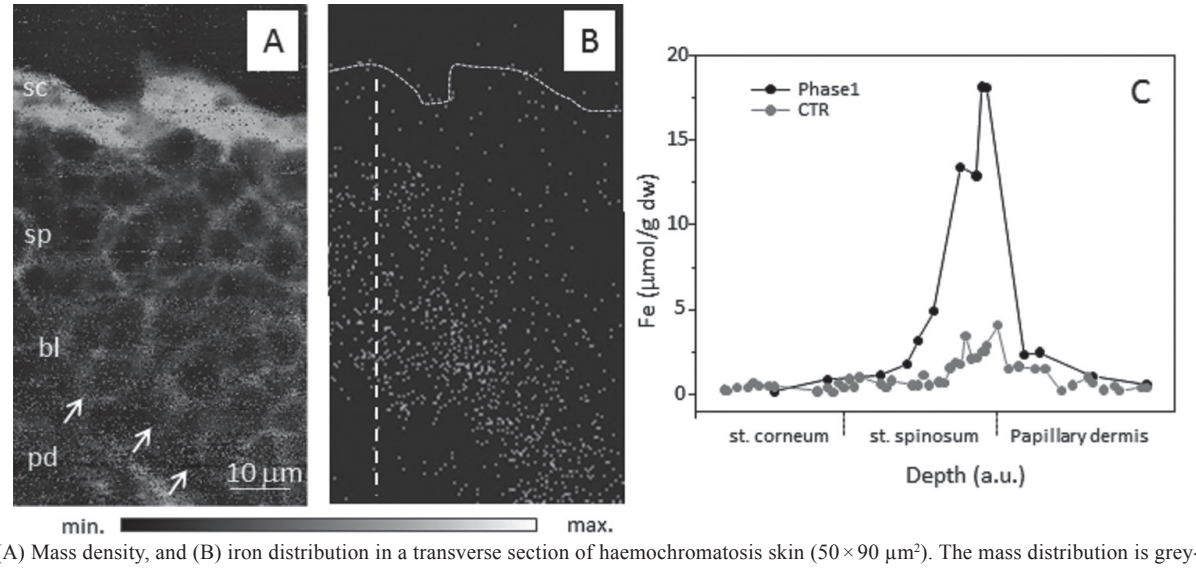

Fig. 1. (A) Mass density, and (B) iron distribution in a transverse section of haemochromatosis skin (50 × 90 μm²). The mass distribution is grey-coded: the highest mass/iron content is coded *white*. The coded images are plotted as a 2-dimensional contour map. The dotted line in B indicates the upper limit of the stratum corneum. sp: stratum spinosum; pd: papillary dermis; arrows: basal layer. (C) Iron profiles, from the outermost layer (stratum corneum) to papillary dermis, as indicated by the vertical dashed line in (B) in skin sections of one patient (Phase 1) and one control skin sample (CTR).

Table I. *Mean iron concentrations (µmol/g dry weight) in control skin (17, 20) and in patients with hereditary haemochromatosis, measured at diagnosis, end of the phlebotomy programme, and 6 months after the end of the programme (Phase 1, 2 and 3, respectively)*

	Control	Phase 1	Phase 2	Phase 3
Stratum corneum	1.25 ± 0.32	1.54 ± 0.32	0.83 ± 0.20	1.50 ± 0.75
Stratum spinosum	0.49 ± 0.06	1.44 ± 0.32*,a,c	0.59 ± 0.08	0.55 ± 0.08
Basal layer	1.77 ± 0.46	7.33 ± 0.98*,a,c	2.71 ± 0.36*	2.08 ± 0.36
Papillary dermis	0.98 ± 0.30	3.00 ± 0.50*,a,c	1.78 ± 0.44*	1.89 ± 0.60*
Total epidermis	0.98 ± 0.30	4.10 ± 0.56*,a,c	1.58 ± 0.22*,b	1.18 ± 0.20*
Superficial skin	0.98 ± 0.26	3.81 ± 0.42*,a,c	1.64 ± 0.20*	1.35 ± 0.22*

*Significantly different from controls; [a]significant difference between Phase 1 and Phase 2; [b]significant difference between Phase 2 and Phase 3; [c]significant difference between Phase 1 and Phase 3.

under the light microscope (bright-field and/or dark-field reflection microscopy) prior to analysis, in order to assess cell overlap and cell sizes. In frozen-hydrated tissues, cells above the basal membrane ranged from 10 µm to 15 µm in diameter, corresponding approximately to the section thickness (14 µm). The tissue contracted slightly after the freeze-drying procedure, as observed in Fig. 2. Fig. 2 shows a mass density image of keratinocytes lying above the basal cells and the corresponding iron map. Iron deposits within the extracellular and cell membrane compartments can be observed. In phlebotomy naïve patients, extracellular iron concentration significantly exceeded the intracellular content (10.3 ± 1.3 µmol/g vs. 4.8 ± 0.9 µmol/g; $p < 0.001$). At Phases 2 and 3 the iron concentrations inside and outside the cells diminished remarkably. However, the extracellular rate of iron clearance was lower than that of intracellular clearance. At Phase 2, the extracellular iron concentration was 2.2-fold higher than that inside the cells (2.8 ± 2.2 µmol/g vs. 1.3 ± 1.0 µmol/g; $p = 0.02$) and, at Phase 3, the ratio increased to 3.2 (2.7 ± 2.0 µmol/g vs. 0.9 ± 0.5 µmol/g; $p < 0.001$).

Modifiers of iron concentrations in the skin

Iron concentrations in HH skin (whether considering major components or individual strata) were not dependent on sex or gender. Also, co-morbidities did not influence iron concentration in the skin. The genotype was significantly associated with iron concentration in the skin only at Phase 1[2].

Relationship between concentration of iron in the skin, blood indicators, and concentration of iron in the liver

At Phase 1, the concentration of iron in all regions of HH skin was correlated with blood TS, Ferr and P-Fe ($p < 0.05$). S-Fe did not correlate with EPI and SSK iron content. A strong correlation was found between LIC and SP, BL, EPI and SSK ($p < 0.001$). The decrease in LIC was comparable with that in skin, showing a progressive and significant decline up to 6 months after stopping the therapy programme. By contrast, data might suggest a trend towards an increase in Ferr, TS, SFe and PFe iron levels at Phase 3 (Table SII[1]).

Despite different LIC and SSK values, a 2.2-fold iron content decrease was observed in going from Phase 1 to Phase 2, but this decrease was limited to 1.2-fold between Phase 2 and Phase 3 in both organs (values are shown in Tables I and SII[1])[3].

Overall, it can be deduced that the iron concentration in BL, EPI and SSK was correlated with LIC throughout the treatment and follow-up. Iron content in the skin was correlated with Ferr and TS only in non-treated patients.

Significance of time-dependent iron content changes studied by regression analysis

The overall iron contents of the skin and the liver were significantly correlated (Fig. 3). The changes in iron concentration as a function of time for all patients in

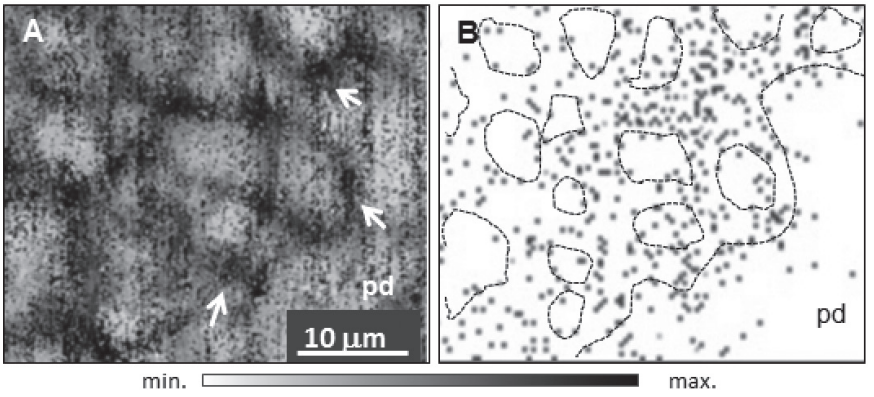

Fig. 2. (A) High-resolution image of lower epidermis region showing a few cells likely to be keratinocytes in the basal layer (*arrows*) above papillary dermis (pd). (B) Corresponding iron map (32 × 38 µm²). The cell contours and basal layer limit (*dotted lines*) taken from mass density image were added to the iron map to facilitate interpretation. The highest mass density and iron content are coded black.

[2]Patients with single H63D mutation had significantly higher iron concentrations in BL, EPI and SSK ($n = 5$; BL = 7.7 ± 1.6 µmol/g; EPI = 5.3 ± 0.9 µmol/g; SSK = 4.7 ± 0.7 µmol/g) than C282Y homozygous patients ($n = 14$; BL = 5.8 ± 1.4 µmol/g; EPI = 3.9 ± 1.1 µmol/g; SSK = 3.3 ± 0.8 µmol/g) or C282Y heterozygous ($n = 9$; BL = 4.6 ± 0.8 µmol/g; EPI = 2.9 ± 0.7 µmol/g; SSK = 2.8 ± 0.6 µmol/g). However, the decrease in iron concentration during Phase 2 and the follow-up does not depend on the genotype.

[3] Similar rate of decrease in the iron content was observed with individual stratum, ranging from 1.7 in PD to 2.4 in BL between Phases 1 and 2 and from 1.4 in BL to 0.9 in SC and PD between Phases 2 and 3. The iron content decrease in BL, EPI, SSK and liver from Phase 1 to Phase 2 and Phase 3 was also correlated with the amount of iron removed during therapy ($p < 0.05$).

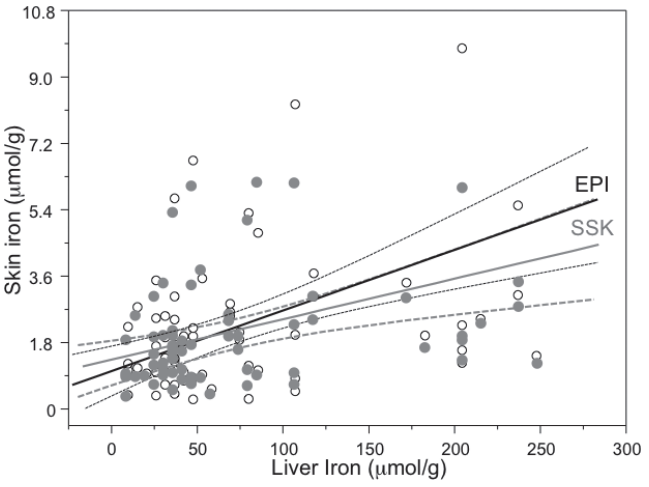

Fig. 3. Relationship between iron concentration in the skin and the liver in patients with hereditary haemochromatosis. Solid lines: regression for total epidermis (EPI); and superficial skin (SSK). Dashed lines: corresponding 95% confidence intervals (EPI: skin iron = 44+0.97*LIC, $r = 0.448$, $p = 0.0001$; SSK: skin iron = 66+0.66*LIC, $r = 0.39$, $p = 0.0009$).

SP, BL, EPI and SSK, from Phase 1 to Phase 2 and to Phase 3 were highly significant ($p < 0.001$)[4]. While the amount of iron removed is marginally correlated with the decrease in concentration of iron in the skin in going from Phase 1 to Phase 2 ($p = 0.07$), a high statistical significance is obtained with Phase 3, which reflects the therapeutic effect[5].

DISCUSSION

The present work demonstrates that, in patients with primary HH, the iron content of epidermis, reflects iron overload in the liver. Although LIC is now rarely determined through invasive liver biopsies, but rather by MRI measurements, it is worth noting that iron assessment by MRI may be influenced by tissue condition and relaxation properties of the tissue iron (20). Although iron deposition occurs in dermis around adnexal structures, the nuclear microscopy imaging demonstrates that the BL is the preferential site of uniform iron deposition in the skin, and is therefore adequate for quantitation purposes. This method has the unique capability to provide real-time morphological images, maps of multiple elements and, simultaneously, to quantify them down to the level of parts per million. Iron determination in skin sections can be achieved rapidly, in approximately 2 h; thus this method can be used routinely. It is therefore a powerful research tool for dermatology (16, 19), allowing precise follow-up of the clearance of iron from tissues during phlebotomy therapy.

The BL is the most metabolically active region of the skin, where cell proliferation and differentiation occur, iron being indispensable for these processes. Even in control skin, the iron content in the BL is higher than that in other parts of the skin. Interestingly, nuclear imaging demonstrates that iron is found preferentially in the extracellular space or bound to cell membrane. In addition, data obtained with this method suggest that the iron concentration in BL, EPI and SSK is correlated with the circulating ferritin content.

The apparent discrepancy between our results in HH epidermis and those described in the experimental mouse model by Adams et al. (15) is probably related to the skin isolation procedure, which may wash away most of the extracellular iron.

The consequence of the excess iron distribution in the skin of patients with HH must be discussed in the light of cell iron metabolism. In all cells, iron uptake and storage are tightly regulated to guarantee sufficient iron for essential cellular processes and to prevent the production of damaging free radicals. In hepatocyte membrane, it is hypothesized that a homozygous C282Y mutation of the HFE gene prohibits the assembly of the transferrin-receptor 1 (TFR1) with the HFE protein, thereby compromising the cellular influx of transferrin-bound iron from the endosomal compartment to the cytosol (21, 22).

The iron-binding capacity of transferrin in the plasma of patients with HH is often exceeded. In this study, 14 out of 28 patients had 70% or more transferrin saturation. Non-transferrin-bound iron is present as low-molecular-mass iron complexes of citrate and acetate (23, 24). These low-molecular-mass complexes can initiate free radical damage as they supply iron ions in a form capable of accelerating free radical reactions and lipid peroxidation (25). In this regard, iron sensitizes cultured human skin fibroblasts to the ultraviolet A (UVA) radiation when cells are treated with low molecular mass complexes or exposed to high ferritin and holotransferrin concentrations with evidence of increased membrane lipid peroxidation and cytotoxicity (26) and activation of MAP kinases (27). The present study, showing that the extracellular space is the major site of excess iron deposition in the skin of patients with HH (Figs 1B and 2), might provide evidence about the lack of notable UVA-induced skin sensitization.

Genotype may contribute to iron overload with variable penetrance and phenotypic expression may be

[4]The changes in SP, BL, EPI and SSK iron content with time were associated with changes in LIC ($p < 0.05$), the EPI variations being the most significant ($p = 0.008$). The decrease in Ferr content was correlated with the iron content decrease in BL ($p = 0.001$), SP ($p = 0.003$) and EPI ($p = 0.002$) showing a steeper mean trend in the decrease in iron content in going from Phase 1 to Phase 2. However, incorporating TS, PFe and SFe values into the regression models used with skin failed to be significant in going from Phase 1 to Phases 2 and 3. This means that the levels of these indicators do not contribute to the mean trend of change in iron concentration in the skin.

[5]It is of note that the genotype did not influence changes in skin iron as a function of time. By contrast, in the case of LIC, the average slope of the mean rate of decrease in iron content was significantly modified in the C282Y genotype $p = 0.021$). In liver, the iron changes during therapy were also correlated with the Ferr ($p = 0.05$) and TS ($p = 0.003$) levels in blood.

influenced by cofactors (8, 28–30) and other additive individual factors (1, 5, 28). It is therefore reasonable to observe a lack of significance in the correlation between iron blood indicators and body stores, such as skin and liver over a long time-period. This raises the possibility that, in some cases, there is a differential cellular iron handling, which results in variable accumulation of iron (5, 6, 8, 15, 28–30).

ACKNOWLEDGEMENTS

The work was carried out under Portuguese Society of Dermatology and Venereology (SPDV) and IAEA RC 302-F1.20.19-POR-13262 research contracts. The reference group for skin was established under the research contract EC/QLK4-CT-2002-02678.

REFERENCES

1. Allen KJ, Gurrin LC, Constantine CC, Osborne NJ, Delatycki MB, Nicoll AJ, et al. Iron-overload-related disease in HFE hereditary hemochromatosis. N Engl J Med 2008; 358: 221–230.
2. Brissot P, Troadec M-B, Bardou-Jacquet E, Le Lan C, Jouanolle A-M, Deugnier Y, et al. Current approach to hemochromatosis. Blood Rev 2008; 22: 195–210.
3. Chevrant-Breton J, Simon M, Bourel, Ferrand B. Cutaneous manifestations of idiopathic hemochromatosis. Study of 100 cases. Arch Dermatol 1977; 113: 161–165.
4. Feder JN, Penny DM, Irrinki A, Lee VK, Lebrón JA, Watson N, et al. The hemochromatosis gene product complexes with the transferrin receptor and lowers its affinity for ligand binding. Proc Natl Acad Sci USA 1998; 95: 1472–1477.
5. Aranda N, Viteri FE, Montserrat C, Arija M. Effects of C282Y, H63D, and S65C HFE gene mutations, diet, and life-style factors on iron status in a general Mediterranean population from Tarragona, Spain. Ann Hematol 2010; 89: 767–773.
6. Cheng R, Barton JC, Morrison ED, Phatak PD, Krawitt EL, Gorgon SC, et al. Differences in hepatic phenotype between hemochromatosis patients with HFE C282Y homozygosity and other HFE genotypes. J Clin Gastroenterol 2009; 43: 569–573.
7. Bacon BR, Adams PC, Kowdley KV, Powell LW, Tavill AS. Diagnosis and management of hemochromatosis: 2011 practice guideline by the American Association for the Study of Liver Disease. Hepatology 2011; 54: 328–343.
8. Sebastiani G, Wallace DF, Davies SE, Kulhalli V, Walker AP, Dooley JS. Fatty liver in H63D homozygotes with hyperferritinemia. World J Gastroenterol 2006; 12: 1788–1792.
9. Alústiza JM, Castiella A, De Juan MD, Emparanza JI, Artetxe J, Uranga M. Iron overload in the liver diagnostic and quantification Eur J Radiol 2007; 61: 499–506.
10. Dereure O, Jumez N, Bessis D, Gallix B, Guillot B. Measurement of liver iron content by magnetic resonance imaging in 20 patients with overt porphyria cutanea tarda before phlebotomy therapy: a prospective study. Acta Derm Venereol 2008; 88: 341–345.
11. Beamish MR, Jobbins K, Cavill I. The cellular distribution of transferrin-bound iron in the skin. Br J Dermatol 1971; 85: 49–51.
12. B. Forslind. The skin barrier: analysis of physiologically important elements and trace elements. Acta Derm Venereol 2000; 208: 46–52.
13. Youssry I, Mohsen NA, Shaker OG, El-Hennawy A, Fawzy R, Abu-Zeid NM, et al. Skin iron concentration: a simple, highly sensitive method for iron stores evaluation in thalassemia patients. Hemoglobin 2007; 31: 357–365.
14. Farquharson MJ, Bagshaw AP, Porter JB, Abeysinghe RD. The use of skin Fe levels as a surrogate marker for organ Fe levels, to monitor treatment in cases of iron overload. Phys Med Biol 2000; 45: 1387–1396.
15. Adams BD, Lazova R, Andrews NC, Milstone LM. Iron in skin of mice with three etiologies of systemic iron overload. J Invest Dermatol 2005; 125: 1200–1205.
16. Verissimo A, Alves LC, Filipe P, Silva JN, Silva R, Ynsa MD, et al. Nuclear microscopy: a tool for imaging elemental distribution and percutaneous absorption in vivo. Microscopy Res Tech 2007; 70: 302–309.
17. Barreiros A, Pinheiro T, Araújo MF, Costa MM, Palha M, da Silva RC. Quality assurance of X-ray spectrometry for chemical analysis. Spectrochimica Acta B 2001; 56: 2095–2106.
18. Gandon Y, Olivié D, Guyader D, Aubé C, Oberti F, Sebille V, et al. Non-invasive assessment of hepatic iron stores by MRI. Lancet 2004; 363: 357–362.
19. Filipe P, Silva JN, Silva R, Cirne de Castro JL, Marques Gomes M, Alves LC, et al. Stratum corneum is an effective barrier to TiO2 and ZnO nanoparticle percutaneous absorption. Skin Pharmacol Physiol 2009; 22: 266–275.
20. St Pierre TG, Clark PR, Chua-Anusorn W, Fleming AJ, Jeffrey GP, Olynyk JK, et al. Noninvasive measurement and imaging of liver iron concentrations using proton magnetic resonance. Blood 2005; 105: 855–861.
21. Yeh K-Y, Yeh M, Watkins JA, Rodriguez-Paris J, Glass J. Dietary iron induces rapid changes in rat intestinal divalent metal transporter expression. Am J Physiol Gastrointest Liver Physiol 2000; 279: G1070–G1079.
22. Schmidt PJ, Toran PT, Giannetti AM, Bjorkman PJ, Andrews NC. Transferrin receptor modulates Hfe-dependent regulation of hepcidin expression. Cell Metab 2008; 7: 205–214.
23. Hershko, C, Peto TEA. Non-transferrin plasma iron. Br J Haematol 1987; 66: 149–151.
24. Grootveld M, Bell JD, Halliwell B, Aruoma OI, Bomford A, Sadler PJ. Non-transferrin-bound iron in plasma or serum from patients with idiopathic hemochromatosis. J Biol Chem 1989; 264: 4417–4422.
25. Gutteridge J MC, Quinlan GJ. Antioxidant protection against organic and inorganic oxygen radicals by normal human plasma: the important primary role for iron-binding and iron-oxidising proteins. Biochem Biophys Acta 1993; 1156: 144–150.
26. Morlière P, Salmon S, Aubailly M, Risler A, Santus R. Sensitization of skin fibroblasts to UVA by excess iron. Biochem Biophys Acta 1997; 1334: 283–290.
27. Jiang J, Pelle E, Yang Q, Pernodet N, Maes D, Huang X. Iron sensitizes keratinocytes and fibroblasts to UVA-mediated matrix metalloproteinase-1 through TNF-α and ERK activation. Exp Dermatol 2011; 20: 249–254.
28. Machado MV, Ravasco P, Martins A, Almeida MR, Camilo ME, Cortez-Pinto H. Iron homeostasis and H63D mutations in alcoholics with and without liver disease. World J Gastroenterol 2009; 15: 106–111.
29. Poblete-Gutiérrez P, Mendez M, Wiederholt T, Merk HF, Fontanellas A, Wolff C, et al. The molecular basis of porphyria cutanea tarda in Chile: identification and functional characterization of mutations in the uroporphyrinogen decarboxylase gene. Exp Dermatol 2004; 13: 372–379.
30. Toll A, Celis R, Ozalla MD, Bruguera M, Herrero C, Ercilla MG. The prevalence of HFE C282Y gene mutation is increased in Spanish patients with porphyria cutanea tarda without hepatitis C virus infection. J Eur Acad Dermatol Venereol 2006; 20: 1201–1206.